Computer Applications in Electrical Engineering
Vol. 13 *2015*

Analysis of the power losses in the three-phase high-current busducts

Tomasz Szczegielniak, Zygmunt Piątek, Dariusz Kusiak
Częstochowa University of Technology
42-200 Częstochowa, ul. Brzeźnicka 60a, e-mail: zygmunt.piatek@interia.pl, dariuszkusiak@wp.pl, szczegielniakt@interia.pl

This paper presents an analytical method for determining the power losses in the three-phase gas-insulated transmission line (*i.e.*, high-current busduct) of circular cross-section geometry. The mathematical model takes into account the skin effect and the proximity effects, as well as the complete electromagnetic coupling between phase conductors and enclosures (*i.e.*, screens). Apart from analytical calculation, computer simulations for high-current busduct system power losses were also performed with the aid of the commercial FEMM software, using two-dimensional finite elements.

KEYWORDS: high-current busduct, power losses, electromagnetic field

1. Introduction

Following the development of thermal and hydroelectric power stations, at the beginning of the 30s, high-current transmission lines with screened busducts connecting big generators with unit transformers began to be installed. Due to the necessity of transmitting power becoming higher and higher, and to the environmental protection requirements, the length of the line was to be a few kilometers [1-10]. It is estimated that until now the length of the existing lines of that type has not surpassed 100 km. The gas most often used for insulation is SF_6 (sulphur hexafluoride) whose pressure values range from 0.29 to 0.51 MPa (at 20°C). Recently, SF_6 has been replaced with the 95% mixture of nitrogen N_2 and 5% of SF_6 of 1.3 MPa pressure, or with a 90% mixture of nitrogen N_2 and 10% of SF_6 of 0.94 MPa pressure, as well as with a 80% mixture of nitrogen N_2 and 20% of SF_6 of 0.71 MPa pressure corresponding to the 0.4 MPa pressure in the case when pure SF_6 is used [8-10]. The contemporary solutions consist of transmission lines insulated with air at atmospheric pressure, with duty-rated voltage values reaching up to 36 kV and duty-rated current values reaching up to: 10 kA for hydroelectric power plants, 20 kA for thermal and nuclear plants whose duty-rated power values reach up to 900 MW, 31.5 kA for nuclear plants with power value of 1300 MW [8-10]. Today high-current busducts are applied in many projects around the world when high-power transmission of high

reliability and maximum availability is required. The sizes of new projects are constantly increasing: from some hundred meters to several kilometers [8-10].

The most popular shielded three-phase high-current busducts are depicted in Figure 1 and 2.

Fig. 1. Three-pole high-currents busduct [11]

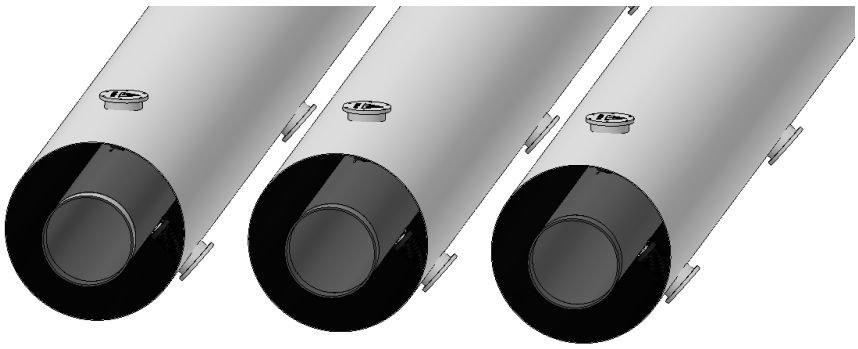

Fig. 2. Single-pole high-currents busduct [11]

Power losses depend on value of currents, and for the large cross-sectional dimensions of the phase conductor, even at industrial frequency, skin, external (Fig. 3) and internal (Fig. 4) proximity effect should be taken into account [1-7].

2. Power losses

The electromagnetic field and the power losses produced by high-current busducts are usually calculated numerically with the use of a computer [9,10]. However, the analytical calculation of these parameters is preferable, because it results in a mathematical expression for showing its dependences on various parameters of the line arrangement [1-8].

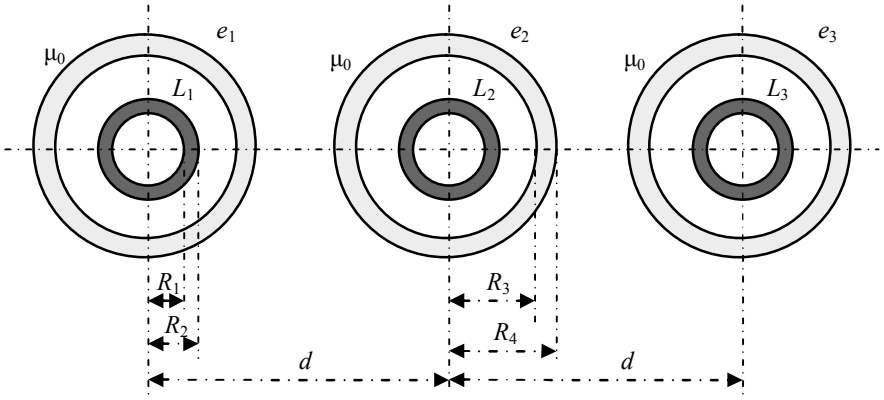

Fig. 3. Single-pole three-phase high-current busduct

Using the Laplace's and Helmoltz's equations we can determine the electromagnetic field in the conductors and the screens for single and three-pole high current busducts [1, 2]. In the case of three-phase single-pole high-current busduct shown in Figure 3 the power losses in the phase conductors is [7]

$$P_L = \frac{\underline{\Gamma}\, l\, I_1^2}{4\,\pi\,\gamma\,R_2}\,\frac{\underline{a}}{\underline{b}\,\underline{b}^*} \tag{1}$$

In turn, power losses in the outer screens (e_1 and e_3) are the same and can be write down as follows:

$$P_{s13} = P_{e0} + P_{e13} \tag{2}$$

where

$$P_{e0} = \frac{\underline{\Gamma}_e^*\, l\, I_1^{\,2}}{4\,\pi\,\gamma_e\,\beta_e^2\,R_4}\,\frac{\underline{a}_0}{\underline{d}_0\,\underline{d}_0^*} \tag{2a}$$

$$P_{e13} = \frac{\underline{\Gamma}_e^{\,*}\, l\, I_1^2}{2\,\pi\,\gamma\,R_4}\sum_{n=1}^{\infty} A_n^2\left(\frac{R_4}{d}\right)^{2n}\frac{\underline{a}_{ne}}{\underline{b}_{ne}\,\underline{b}_{ne}^*} \tag{2b}$$

in which

$$\underline{A}_n = -\frac{1}{2}\left[\left(1+2^{-n}\right)+\mathrm{j}\sqrt{3}\left(1-2^{-n}\right)\right] \tag{2c}$$

Power losses in the middle screen (e_2) are

$$P_{s2} = P_{e0} + P_{e2} \tag{3}$$

in which

$$P_{e2} = \frac{\underline{\Gamma}_e^{\,*}\, l\, I_1^2}{2\,\pi\,\gamma\,R_4}\sum_{n=1}^{\infty} B_n^2\left(\frac{R_4}{d}\right)^{2n}\frac{\underline{a}_{ne}}{\underline{b}_{ne}\,\underline{b}_{ne}^*} \tag{3a}$$

and

$$\underline{B}_n = \frac{1}{2}\left\{-\left[(-1)^n + 1\right] + \mathrm{j}\sqrt{3}\left[(-1)^n - 1\right]\right\} \tag{3b}$$

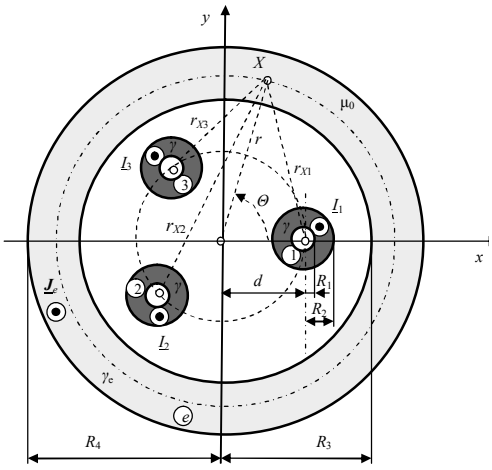

Fig. 4. Three-pole three-phase high-current busduct

For the three-pole high-current busduct (depicted in the Figure 4) the power losses of the phase conductors are the same and can be write down as follows [3]:

$$P_{L123} = P_L + P_{123} \tag{4}$$

where

$$P_{123} = \frac{\underline{\Gamma}^* \, l \, I_1^2}{2\,\pi^2\,\gamma\,R_2} \sum_{n=1}^{\infty}\left(\int_0^{2\pi} D_n^2 \,\mathrm{d}\Theta\right)\left(\frac{R_2}{d}\right)^{2n} \frac{\underline{a}_n}{\underline{b}_n\,\underline{b}_n^*} \tag{4a}$$

and

$$\underline{D}_n = \exp\left[-\mathrm{j}\frac{2}{3}\pi\right]\cos n\Theta + \exp\left[\mathrm{j}\frac{2}{3}\pi\right]\cos n\left(\Theta - \frac{\pi}{3}\right) \tag{4b}$$

Power losses in the screen of the three-pole high-current busduct (presented in the figure 4) are expressed by formula [3]

$$P_s = \frac{l\,\underline{\Gamma}_\mathrm{e}^{\,*}\,I_l^{\,2}R_4}{2\pi\gamma_\mathrm{e}\;R_3^{\,2}} \sum_{n=1}^{\infty}\frac{9}{2}\pi\left(\frac{d}{R_3}\right)^{2n}\frac{\underline{a}_{nn}}{\underline{d}_n\,\underline{d}_n^{\,*}} \tag{5}$$

Parameters $\underline{a}$, $\underline{a}_0$, $\underline{a}_n$, $\underline{a}_{ne}$, $\underline{a}_{ne}$, $\underline{b}$, $\underline{b}_n$, $\underline{b}_{ne}$, $\underline{d}_0$, $\underline{d}_n$ are expressed by Bessel's functions and presented in the papers [2-7], but the complex propagation constant of electromagnetic wave in the conductor equals

$$\underline{\Gamma} = \sqrt{\mathrm{j}\omega\mu_0\gamma} = \sqrt{\omega\mu_0\gamma}\,\exp[\mathrm{j}\frac{\pi}{4}] = k + \mathrm{j}\,k = \sqrt{2\mathrm{j}}\,k \tag{6}$$

with the attenuation constant

$$k = \sqrt{\frac{\omega \mu_0 \gamma}{2}} = \frac{1}{\delta} \tag{7}$$

where δ is the electrical skin depth of the electromagnetic wave penetration into the conducting environment, ω is the angular frequency, γ stands for the conductivity of conductor, and $\mu_0 = 4\pi\,10^{-7}\ \mathrm{H \cdot m^{-1}}$ is the magnetic permeability of the vacuum.

The complex propagation constant in the screen is $\underline{\Gamma}_e = \sqrt{\mathrm{j}\omega\mu_0\gamma_e}$, and γ_e is the conductivity of the screen.

3. Numerical example

Based on the derived formulae, the power losses in the high-current busduct depicted in Figure 3 and 4 were calculated. Calculations were made for high-current busducts produced by Holduct (for models: EHON-12/2 and HOIO-24/2). According to the notation applied in Figure 3, the following geometry of the busduct has been selected: $R_1 = 30$ mm, $R_2 = 40$ mm, $R_3 = 230$ mm, $R_4 = 240$ mm, $d = 640$ mm. For the busduct depicted in figure 4, the geometrical parameters are: $R_1 = 30$ mm, $R_2 = 40$ mm, $R_3 = 230$ mm, $R_4 = 240$ mm, $d = 100$ mm. Both the phase conductors and the screen are made of aluminium, which has an electric conductivity of $\gamma = 35\ \mathrm{MS \cdot m^{-1}}$. The frequency is 50 Hz. The length of the busduct system is assumed to be $l = 10$ m. Currents in the phase conductors are $\underline{I}_1 = 2000\exp[-\mathrm{j}\,0]\,\mathrm{A}$, $\underline{I}_2 = 2000\exp[-\mathrm{j}\frac{2}{3}\pi]\,\mathrm{A}$, $\underline{I}_3 = 2000\exp[\mathrm{j}\frac{2}{3}\pi]\,\mathrm{A}$. The results of the calculations are shown in Tables 1 and 2.

Table 1. Power losses of the three-pole high-current busduct depicted in Figure 4

Method	P (W)			
	L_1	L_2	L_3	Screen
Analytical	523.447	523.447	523.447	164.912
FEMM	565.078	565.04	565.037	148.818

Apart from analytical calculation, computer simulations for high-current busduct system power losses were also performed with the aid of the commercial FEMM software [12], using two-dimensional finite elements. Figure 5 shows the computational finite element mesh for three-pole high-current busduct.

Table 2. Power losses of the single-pole high-current busduct depicted in Figure 3

Method	P (W)					
	L_1	L_2	L_3	Screen e_1	Screen e_2	Screen e_3
Analytical	538.328	538.328	538.328	44.789	117.664	44.789
FEMM	546.21	546.225	546.179	43.887	110.065	41.67

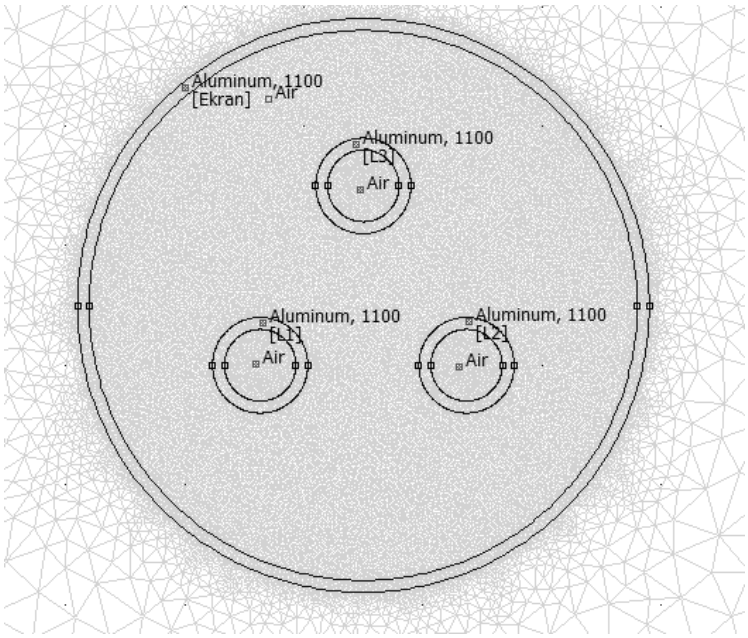

Fig. 5. The finite element mesh used in FEMM computations

4. Conclusions

An analytical approach to the solution of the power losses in the three-phase high-current busduct has been presented in this paper. The proposed method allows us to calculate the power losses in a set tubular busbars. The mathematical model takes into account the skin effect and the proximity effects, as well as the complete electromagnetic coupling between phase conductors and screens. To verify the analytical formulae we performed computations by means of the finite element method.

As Tables 1 and 2 show, the power losses calculated on the basis analytical formulae and power losses determined by FEMM software are different both for single-pole and three-pole high-current busduct. These differences could be caused scarce of the finite element mesh used in FEMM computations.

An analytical method presented in the paper can be used only for circular high-current busducts. But numerical method can be used almost for all types of busducts.

References

[1] Nawrowski R.: Tory wielkoprądowe izolowane powietrzem lub SF_6. Wyd. Pol. Poznańskiej, Poznań 1998.

[2] Piątek Z.: Impedances of high-current busducts. Wyd. Pol. Częst., Czestochowa 2008.

[3] Szczegielniak T.: Straty mocy w nieekranowanych i ekranowanych rurowych torach wielkoprądowych, Praca Doktorska, Gliwice, 2011.

[4] Piątek Z., Szczegielniak T., Kusiak D.: Power losses in the screens of the symmetrical three phase high current busduct, Computer Applications in Electrical Engineering. Ed. by Ryszard Nawrowski, Poznań 2012.

[5] Piątek Z ., Szczegielniak T., Kusiak D.: Wpływ zewnętrznego zjawiska zbliżenia na straty mocy w trójfazowym płaskim torze wielkoprądowym, XVI Conference Computer Applications in Electrical Engineering, s 15-16 Poznań 2011.

[6] Piątek Z., Szczegielniak T., Kusiak D.: Straty mocy w ekranach trójfazowego jednobiegunowego toru wielkoprądowego, Electrical Engineering, Iss.73, s.91-98, 2013.

[7] Szczegielniak T., Kusiak D., Jabłoński P., Piątek Z.: Power losses in a three-phase single-pole gas-insulated transmission line (GIL), International Review of Electrical Engineering (IREE), October 2013, Vol. 8, N. 5.

[8] Koch, H.: Gas-Insulated Transmission Lines (GIL). John Wiley & Sons, 2012.

[9] CIGRE TB 218.: Gas Insulated Transmission Lines (GIL, CIGRE, Paris, France, 2003.

[10] CIGRE TB 351.: Application of Long High Capacity Gas Insulated Lines (GIL), CIGRE, Paris, France, 2008.

[11] Holduct – Z. H. Ltd. Polska.: Szynoprzewody trójfazowe okrągłe. [Online]. Available: http://www.holduct.com.pl/index.php?menu=p2

[12] Meeker, D.C., Finite Element Method Magnetics, version 4.2 (11apr2012, Mathematica Build), http://www.femm.info.

(Received: 4. 10. 2015, revised: 11. 12. 2015)